Graphical Abstract

Adsorption behavior of associating nanoparticle-polymer systems in the vicinity of an attractive surface: Predictions from classical density functional theory

Debadutta Prusty, Alejandro Gallegos, Jianzhong Wu

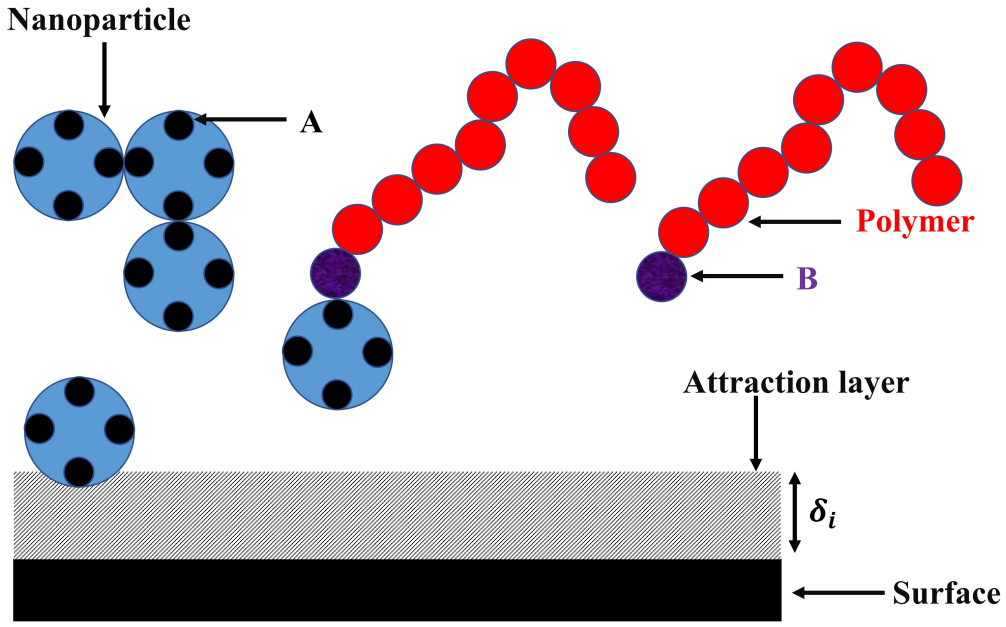

Highlights

Adsorption behavior of associating nanoparticle-polymer systems in the vicinity of an attractive surface: Predictions from classical density functional theory

Debadutta Prusty, Alejandro Gallegos, Jianzhong Wu

- Adsorption behavior of an associative nanoparticle-polymer mixture onto an attractive surface has been investigated with classical density functional theory for inhomogeneous fluids.
- Increasing nanoparticle-nanoparticle association strength promotes nanoparticle adsorption while increasing nanoparticle-polymer association strength leads to suppression of adsorption.
- There is a coupling between nanoparticle adsorption and polymer chain properties such as its chain length and surface affinity.
- The case of surface with saturable surface groups is incorporated into the formalism, wherein a different effect of nanoparticle-nanoparticle association strength is observed.

Adsorption behavior of associating nanoparticle-polymer systems in the vicinity of an attractive surface: Predictions from classical density functional theory

Debadutta Prusty, Alejandro Gallegos, Jianzhong Wu[1,]

[a]*Department of Chemical and Environmental Engineering, University of California Riverside, 92507, California, USA*

Abstract

Interfacial behavior of associating species is important both from a fundamental physics perspective and from an industrial application point of view. Specifically, in the petroleum industry, self-association between asphaltene molecules causes them to aggregate and subsequently deposit on various surfaces, reducing the efficacy of oil extraction. Presence of surfactant-like molecules such as resins has been shown to inhibit asphaltene aggregation. A coarse-grained model parameterizing all the structural and chemical features of asphaltene and resin would facilitate an understanding of physical principles behind the deposition behavior and guide mitigation strategies. To this end, we investigate the adsorption behavior of a mixture of nanoparticles and polymer chains onto an attractive surface through a classical density functional theory. Representing asphaltenes by nanoparticles and resins by polymer chains, we consider both nanoparticle-nanoparticle self-association and nanoparticle-polymer cross-association. We study the effect of the various chemical and physical characteristics of molecules such as association strengths, the chain length, the surface affinities and the nature of the surface on the adsorption amount of both nanoparticles and polymer molecules. We find that increasing nanoparticle-nanoparticle self-association strength increases nanoparticle adsorption. Conversely, increasing nanoparticle-polymer interaction strength decreases nanoparticle adsorption. We also observe an inverse correlation between polymer chain length and nanoparticle adsorption. We rationalize the observed trends in light of interplay between dif-

Email address: jwu@engr.ucr.edu (Jianzhong Wu)

ferent entropic and energetic driving forces operative in the system. Finally, we present an alternative framework where surface groups creating attraction are saturable and find that unlike adsorption onto an unsaturable surface, increasing nanoparticle-nanoparticle strength can inhibit nanoparticle adsorption.

Keywords: Classical density functional theory, associating nanoparticles, surface affinity

---

1. Introduction

Asphaltenes are heavy components of crude oil that are insoluble in alkanes and soluble in aromatic solvents. These molecules tend to associate among themselves, precipitating into large clusters[1]. This process has been shown to cause operational issues across the entire production chain in oil extraction through changes in wettability of oil, plugging of rock pores and clogging of pipelines [2, 3, 4, 5]. Since asphaltenes are also surface-active in nature, they can deposit on various surfaces (referred to as adsorbents in the text) such as well surfaces and refining equipment [6], imposing heavy financial penalties on the industry through higher equipment maintenance and replacement demands. In this regard, a common mitigation strategy employed is to use the resin content in oil as a controlling parameter on asphaltene segregation. Resins are structurally characterized by alkyl chains with a polar head group. This polar group chemically interacts with asphaltene molecules in addition to interacting with active surfaces, however it does not interact or very weakly interacts with groups of its own type[7, 8]. This nature of interaction essentially weakens self-association between asphaltene functional groups and their interaction with the surface. For example, resin headgroups can bond with asphaltene functional groups, terminating chain formation of asphaltene molecules[9]. This change in bulk colloidal behavior is also reflected in their interaction with adsorbents. Additionally, resin molecules can compete with asphaltene molecules to some extent for adsorption on surfaces [10]. Aside from association interactions, other characteristics of these molecules and the supporting medium, such as solvent quality, chain length of resins, the concentrations of asphaltene and resin and temperature between molecules also become critical in controlling aggregation behavior and surface interactions[11]. This makes the thermodynamics governing the association and adsorption behavior of asphaltene and resin quite

rich.

Prior investigations on adsorption in asphaltene-resin systems have been primarily experimental, focusing on mapping out adsorption isotherms of asphaltene or/and resins of different crude oil grades on nanoparticle surfaces such as silica [10], hematite [10], alumina [12] and nickel oxide [13]. While these studies reveal many useful trends, the parameter space of the system is quite broad, which renders experimentally obtaining insights into the underlying physio-chemical mechanisms an arduous task. Analytical and computational methods can be an effective means to accomplish this task. In this context, continuum approaches agnostic to any specific system chemistry are quite useful due to lower computational power demanded by them than particle-based methods. For bulk and interfacial fluid systems, classical density functional theory (cDFT) has been a widely used tool to study the phase and interface behavior[14]. In asphaltene-resin systems, the molecular-thermodynamic framework for bulk phase behavior was developed by Wu and coworkers [15, 16], wherein asphaltenes were modelled as hard spheres dotted with sticky sites and resins as polymer chains with a sticky site as one of the end monomers. Using this model, the authors examined the effect of pressure and composition on asphaltene precipitation in a few varieties of crude oil and tank oil and obtained good agreement with experimental data. As for the modelling of deposition behavior of asphaltene-resin mixture on surfaces, to our knowledge, there have been no studies on the exact system reported in the literature. In closely related reports, however, associating hard spheres near both hard and attractive walls have been studied[17]. In these studies, the presence of a surface was shown to alter the association behavior of particles, causing enhanced or suppressed adsorption of particles compared to pure hard spheres depending on the nature of the surface. Extensions of this problem include behavior of mixture of associating and non-associating hard spheres near surfaces[18] and alteration of chemical equilibrium under confinement[19]. When a polymer capable of associating with associating hard spheres is introduced in the system, the presence of a few extra molecular factors such as chain conformational entropy, chain translational entropy and an extra associating group might give rise to non-intuitive trends in adsorption behavior.

With the above facts in mind, in the current contribution, we use a classical density functional theory developed in earlier work [15, 16] to study the adsorption behavior of associating nanoparticle and polymer system in the vicinity of an attractive surface. For simplicity, we assume the binding

energy between surface and adsorbing species to be constant. This shall be referred to as non-saturable adsorption. Alternatively, we also consider the case where binding sites on the surface are limited and hence upon their association with active species, the binding energy decreases. This is termed as saturable adsorption. While the former has been the primary modelling approach in the literature so far, the latter has not received much attention.

We organize the article as follows: In section 2, we describe our classical density functional theory based formulation. In section 3, we present and discuss our results in two parts. In the first part, we focus on non-saturable adsorption where the surface potential on particles is insensitive to the adsorbed amount of particles. Given the vast parameter space in this problem, we consider only a few representative cases with a select few parameters and present the dependence of adsorption on these parameters. We explain these results by analyzing the density and association profiles of involved species. In the second part, we present the results of saturable adsorption. Since our primary focus here is to identify the changes induced by the nature of the surface, we restrict ourselves to one component system, focusing only on nanoparticle adsorption. Finally, we present our conclusions and discuss future extensions of the work in section 4.

2. Methods

The schematic of our system is shown in Figure 1. It consists of a surface in contact with a reservoir of a mixture of nanoparticles (referred to as n) and polymer chains (referred to as P). The latter has a degree of polymerization, N_P. In the bulk solution, the nanoparticle and polymer are maintained at concentrations ρ_n^b and ρ_P^b in a supporting continuous medium at temperature T. This medium only indirectly affects the system thermodynamics through dispersive interactions between particles and a few molecular parameters of nanoparticle and polymer [15, 16]. However, we do not consider the effect of dispersive interactions in this work and use other molecular parameters as variables; so the nature of the medium does not enter our analysis. The nanoparticle is a hard sphere with four identical association sites (referred to as A), and the polymer is a chain of tangentially connected hard spheres with an association site (referred to as B) on one of its end monomers. A sites can associate with themselves and with B sites. The surface exerts a short-range attractive potential on nanoparticles and the end monomer of the polymer chain. The rationale behind assigning attraction to only the end monomer

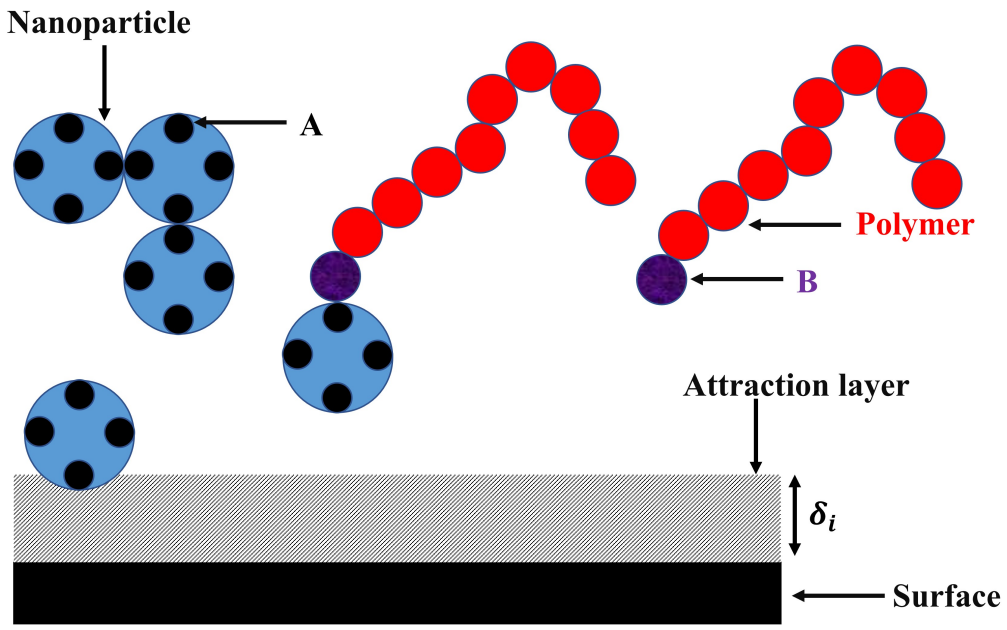

Figure 1: Schematic representation of the nanoparticle-polymer system under study. The black circles on nanoparticles and the purple bead at one of the ends of the polymer chain are the associating functional groups. The white layer of thickness δ_i represents the range of attraction between the surface and species i.

is surface-exerted attraction involves primarily polar forces such as hydrogen bonding or electrostatic interactions [20, 1]. It should be noted that while physical forces such as van der waals interactions can be operative, they are weak compared to polar forces and including them only produces minor quantitative changes in the results. As was mentioned in the introduction, we consider two types of surface interactions a) non-saturable- here, the strength of the interaction is invariant with respect to the adsorbed amount of species b) saturable- where the strength of the interaction is scaled by the fraction of unbonded surfaces sites. The fraction of bonded sites is related to the concentration of adsorbed particles through an equilibrium constant. The mathematical formulation for this phenomenon will be discussed in detail in section 3.3.

We use classical density functional theory to determine the adsorption of nanoparticles on the surface. The central task in cDFT is to find the density profiles of species that minimize the grand potential of the system, expressed

mathematically as:

$$\beta\Omega = \beta F + \beta \int d\mathbf{R}\ \rho_P(\mathbf{R})\{V_P^{ext}(\mathbf{R}) - \mu_P\} + \beta \int d\mathbf{r}\ \rho_n(\mathbf{r})\{V_n^{ext}(\mathbf{r}) - \mu_n\} \quad (1)$$

Here, μ_P and μ_n represent the chemical potentials of the polymer and the nanoparticle, respectively, and $\beta = 1/k_BT$ with k_B standing for Boltzmann constant. $\mathbf{R} = (\mathbf{r}_1, \mathbf{r}_2, ..., \mathbf{r}_N)$ captures the polymer chain configuration and $\rho_P(\mathbf{R})$ is its number density. $\rho_P(\mathbf{R})$ is related to the monomer number density $\rho_m(\mathbf{r})$ of species m by $\rho_m(\mathbf{r}) = \sum_i^{N_m} \int d\mathbf{R}\delta(\mathbf{r} - \mathbf{r}_i)\rho_P(\mathbf{R})$, where the sum is over all monomers of type m, and N_m is the number of such monomers in the chain. $V_{i=m,n}^{ext}(\mathbf{r})$ is the external potential acting on species i due to the surface and is given by:

$$V_i^{ext}(\mathbf{r}) = \begin{cases} \infty, & z < \sigma_i/2, \\ -\epsilon_{is}, & \sigma_i/2 \leq z \leq \delta_i, \\ 0, & z > \delta_i \end{cases} \quad (2)$$

where ϵ_{is} is the strength of attraction, σ_i is the diameter of species i and δ_i is the outer boundary of the attractive layer. In this study, we set δ_i to 1.2 σ_i. In Eqn. (1), the external potential acting on the polymer chain is the sum of the external potential acting on its constituent monomers, that is, $V_P^{ext}(\mathbf{R}) = \sum_{i=1}^{N_P} V_P^{ext}(\mathbf{r}_i)$. For the model systems considered in this work, the Helmholtz free energy contains contributions from various driving forces:

$$\beta F = \beta F^{id} + \beta F^{hs} + \beta F^{ch} + \beta F^{as} \quad (3)$$

In the above equation, βF^{id} is the ideal part of the free energy and is the sum of translational entropy and monomer bond potential.

$$\begin{aligned} \beta F^{id} = &\int d\mathbf{R}\rho_P(\mathbf{R})[[\ln[\rho_P(\mathbf{R})] - 1]] + \int d\mathbf{R}\rho_P(\mathbf{R})\beta V^b(\mathbf{R}) \\ &+ \int d\mathbf{r}\rho_n(\mathbf{r})[\ln[\rho_n(\mathbf{r})] - 1] \end{aligned} \quad (4)$$

where the first and last terms represent the translational entropy of polymer chains and nanoparticles, respectively. For a freely jointed chain, the bond potential $V^b(\mathbf{R})$ is expressed as:

$$\exp[-\beta V^b(\mathbf{R})] = \prod_{i=1}^{N_p - 1} \frac{4}{\pi {\sigma_m}^2} \delta(|\mathbf{r}_{i+1} - \mathbf{r}_i| - \sigma_m) \quad (5)$$

where σ_m is the diameter of monomers. The last three terms in Eqn. (3) constitute the excess free energy terms. βF^{hs} is the free energy of excluded volume interaction among hard spheres of nanoparticles and monomers and is modelled using the modified fundamental measure theory in terms of six weighted densities $(n_0, n_1, n_2, n_3, \mathbf{n}_{V1}, \mathbf{n}_{V2})$[21]:

$$\beta F^{hs} = \int d\mathbf{r}\ \Phi^{hs}(\mathbf{r}) \tag{6}$$

where

$$\begin{aligned}\Phi^{hs}(\mathbf{r}) = &- n_o \ln(1-n_3) + \frac{n_1 n_2 - \mathbf{n}_{V1}\cdot\mathbf{n}_{V2}}{1-n_3} + \\ &\frac{1}{36\pi}[n_3\ln(1-n_3) + \frac{n_3^2}{(1-n_3)^2}]\frac{n_2^3 - 3n_2\mathbf{n_{V2}}\cdot\mathbf{n_{V2}}}{n_3^3}\end{aligned} \tag{7}$$

βF^{ch} is the excess free energy due to connectivity correlations between chain monomers, which is obtained from a generalized first order thermodynamic perturbation theory (TPT1) [22]:

$$\beta F^{ch} = \int d\mathbf{r}\ \frac{(1-N_P)}{N_P}\ n_{oP}\ \zeta_{oP} \ln y(\sigma_m, n_w) \tag{8}$$

where $\zeta_{oP} = 1 - (\mathbf{n^P_{V2}}\cdot\mathbf{n^P_{V2}})/n_{2P}^2$. Here, the weighted densities with P in their subscripts correspond to only chain monomers, and n_w to all species as in Eqn. (7). $y(\sigma_m, n_w)$ is the contact value of the cavity correlation function (CCF) of unconnected chain monomers:

$$y(\sigma_m, n_w) = [\frac{1}{1-n_3} + \frac{n_2\sigma_P(1-\mathbf{n_{V2}}\cdot\mathbf{n_{V2}}/n_2^2)}{4(1-n_3)^2} + \frac{n_2^2\sigma_P(1-\mathbf{n_{V2}}\cdot\mathbf{n_{V2}}/n_2^2)}{72(1-n_3)^3}] \tag{9}$$

The free energy of association is a modification [23] of the free energy of bulk associating fluids [24]:

$$\beta F^{as} = \int d\mathbf{r}\Phi^{as}(\mathbf{r}) \tag{10}$$

where Φ^{as} is given by:

$$\Phi^{as} = n_o\zeta\{4[\ln\chi_A(\mathbf{r}) - \frac{\chi_A(\mathbf{r})}{2} + \frac{1}{2}] + [\ln\chi_{AB}(\mathbf{r}) - \frac{\chi_{AB}(\mathbf{r})}{2} + \frac{1}{2}]\} \tag{11}$$

Here, $\zeta = 1 - (\mathbf{n_{V2}} \cdot \mathbf{n_{V2}})/n_2^2$. $\chi_A(\mathbf{r})$ and $\chi_{AB}(\mathbf{r})$ are the fraction of unassociated nanoparticle functional groups and the fraction of unassociated polymer functional groups, respectively, and are computed from the relations:

$$\chi_A(\mathbf{r}) = (1 + 4\rho_n(\mathbf{r})\triangle^{AA}\chi_A(\mathbf{r}) + \rho_B(\mathbf{r})\triangle^{AB}\chi_{AB}(\mathbf{r}))^{-1} \tag{12}$$

$$\chi_{AB}(\mathbf{r}) = (1 + 4\rho_n(\mathbf{r})\triangle^{AB}\chi_A(\mathbf{r}))^{-1}, \tag{13}$$

where

$$\triangle^{AA} = \sigma_{nn}^3\kappa_{AA}g_{nn}^{hs}(\sigma_{nn}, n_w)[\exp(\beta\epsilon^{AA}) - 1], \tag{14}$$

and

$$\triangle^{AB} = \sigma_{np}^3\kappa_{AB}g_{np}^{hs}(\sigma_{np}, n_w)[\exp(\beta\epsilon^{AB}) - 1] \tag{15}$$

As for bulk systems, κ_{ij} is related to the volume available for bond formation between species i and j functional groups, σ_{nn} and σ_{np} are the average diameters of nanoparticle-nanoparticle and nanoparticle-monomer pairs, and ϵ^{ij} is the the corresponding energy. In our calculations, ϵ_{AA} and ϵ_{AB} are set as variables to study the effect of self-association and inter-association. However, κ_{AA} and κ_{AB} have been set equal to their previously used literature values of 0.05 for asphaltene and resin [15]. $g_{ij}^{hs}(n_w, \sigma_{ij})$ is the local pair correlation function at contact between species i and j given by:

$$g_{ij}^{hs}(n_w, \sigma_{ij}) = \frac{1}{1 - n_3} + \frac{n_2(\sigma_i + \sigma_j)\zeta}{8(1 - n_3)^2} + \frac{n_2^2\sigma_i\sigma_j\zeta}{18(\sigma_i + \sigma_j)^2(1 - n_3)^3} \tag{16}$$

To solve Eqns. 13 and 12, we substitute the latter into the former. This gives a cubic equation in $\chi_A(\mathbf{r})$, which is solved numerically by Newton's method.

To obtain expressions for nanoparticle and polymer density profiles, we substitute the aforementioned individual free energy expressions into Eqn. 1 and minimize the resulting expression with respect to $\rho_n(\mathbf{r})$ and $\rho_P(\mathbf{R})$. This procedure gives

$$\rho_P(\mathbf{R}) = \exp\{\beta[\mu_P - V_b(\mathbf{R}) - \sum_{k=1}^{N_P} w_P^k(\mathbf{r}_P^k)]\} \tag{17}$$

$$\rho_n(\mathbf{r}) = \exp\{\beta[\mu_n - w_n(\mathbf{r})]\} \tag{18}$$

where $w_i(\mathbf{r}) = V_{ext}^i(\mathbf{r}) + \frac{\delta F_{ex}}{\delta\rho_i(\mathbf{r})}$ is the effective field acting on species i.

We solve the above equations only in the z direction, assuming lateral homogeneity. The resulting detailed expressions for the fields, weighted densities and polymer segment profiles are already established in the literature[25] and so we do not restate them here. Picard iteration was used to solve the equations with the boundary condition that far away from the surface the density values of all species approach their bulk concentrations. The stopping criterion was the difference in the bulk-concentration-normalized density values $(\rho_i(z)/\rho_i^b)$ for all species at all locations between two successive iterations must be less than 10^{-3}. In our calculations, we fix the diameters of nanoparticles and monomers to σ_n =1.5 nm and σ_m =0.5 nm, respectively[16]. The chain length was fixed to 10 unless stated otherwise[15, 26]. The molecular weights of the nanoparticle and the polymer of chain length 10 are 2000 and 800, respectively. However, note that these molecular details are dependent on the source of the molecules and we have used agreed-upon average values in the literature. The grid length used in discretization of space was set to 0.05 σ_m.

3. Results and Discussion

The primary quantity of interest in our discussion is the adsorption amount, defined by:

$$\Gamma_{i=n,m} = \int dz[\rho_i(z) - \rho_i^b] \tag{19}$$

and it is expressed in reduced units of $1/{\sigma_n}^2$. Similarly, the bulk density of nanoparticles in the plots is given in terms of their reduced density defined by $\rho^* \equiv 1000\rho_n^b\sigma_n^3$.

3.1. Adsorption in only-nanoparticle system

First, we investigate adsorption in a one component system comprising only nanoparticles, varying their association strength (ϵ_{AA}). As for the surface affinity ($\beta\epsilon_{nS}$) of nanoparticles, we varied it from 2 to 6 and did not see any qualitative change in adsorption isotherms. For the sake of brevity, here we show results only for $\beta\epsilon_{nS} = 2.0$. The left panel in Fig. 2 plots the dependence of Γ_n on bulk nanoparticle concentration for different values of $\beta\epsilon_{AA}$. Since the curves for first five values have become tightly placed due to the abrupt rise in Γ_n for $\beta\epsilon_{AA} = 5$, we provide in the right panel the zoomed-in version of the plot for those small values of $\beta\epsilon_{AA}$. This abrupt rise is due to wetting transition, which we will briefly discuss later in the article.

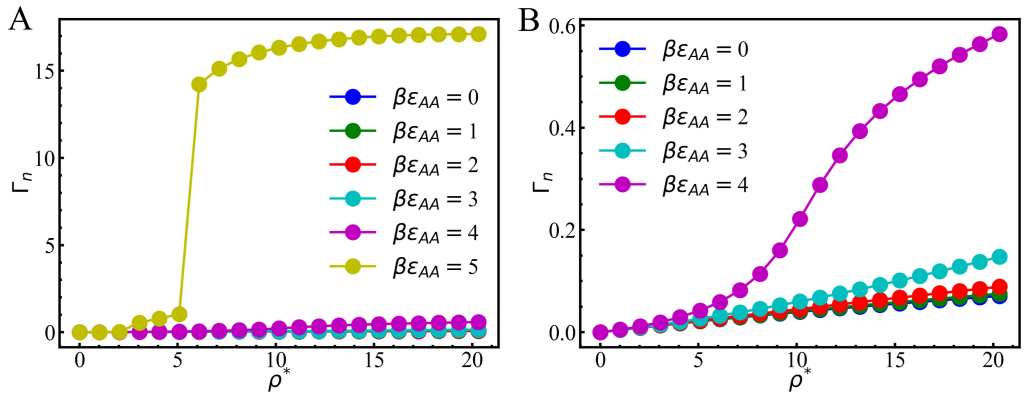

Figure 2: The effect of nanoparticle-nanoparticle association strength ($\beta\epsilon_{AA}$) on nanoparticle adsorption isotherms. The nanoparticle surface affinity is $\beta\epsilon_{nS} = 2.0$. The left panel (A) shows the isotherms for all studied values of $\beta\epsilon_{AA}$, and the right panel (B) is the magnified portion of (A), for the first five $\beta\epsilon_{AA}$ values.

Returning to the results, the plots clearly indicate a positive correlation between the nanoparticle adsorption amount and the association strength. This behavior can be understood by invoking the factors driving the structural organization of particles near a wall. First, a particle near a wall experiences reduced collision from other particles compared to a particle in the bulk due to absence of particles on the wall side. This collision factor has the effect of segregating particles against the wall [17]. Second, bringing particles into the vicinity of a wall results in reduced translational entropy analogous to counterion confinement in polyelectrolyte brushes [27], which acts against their surface segregation. For hard sphere fluids near a hard wall, the former factor dominates the driving force and enrichment of particles near the wall is observed [17]. When an attractive interaction is introduced between particles, the presence of a surface constrains the association between particles by making the side of the particles facing the surface unavailable for binding. This results in a decreased concentration of associating particles near a hard wall with increasing association strengths[17]. However, when the wall is made attractive towards the particles as considered in the current work, gathering of particles against the surface is accompanied by a reduction in system free energy. Additionally, increasing the association energy increases the cluster size of nanoparticles. Intuitively, these clusters can be viewed as polymer chains and hence their increased size compared to unassociated

particles translates to a lower translational entropic cost of confinement. We also note that piling of these clusters near the wall involves a loss in orientational entropy. However, the translational entropic factor coupled with the energy gain overcomes the penalty linked to decreased association near the surface and the orientational entropy and one sees the enrichment of particles near the surface.

To provide quantitative evidence for the surface effect on particle association, we plot in Fig. 3 the association profiles, $(1-\chi_A(z))$, of nanoparticles against the distance from the surface. Here, in addition to enhanced association in the bulk with increasing ϵ_{AA}, the effect is much more significant near the wall because of the enrichment of nanoparticles. In other words, presence of an attractive surface results in increased concentration of nanoparticles near the wall (see density profiles in Fig. 4) and this increased concentration means a nanoparticle functional group has more neighbors to bond with than in the bulk. This explains the dramatic rise in association near the wall in the observed plots in spite of the previously mentioned geometrical constraint on association. This increased association further pulls more nanoparticles towards the surface due to decreased translational entropy of resulting clusters. Therefore, a feedback mechanism between concentration and association near the wall sets in, resulting in the observed behavior in Fig. 2.

When $\beta\epsilon_{AA}$ is increased from 4 to 5, we note an abrupt jump in Γ_n with ρ^* near $\rho^* = 6.0$ (approximately by a factor of 400). In the literature, such behavior has been attributed to wetting transition, where a thick macroscopic layer of absorbing species forms on the surface [28]. Wetting transition has been shown to occur when the bulk concentration of the absorbing species approaches the phase coexistence curve of the bulk fluid between a liquid-like phase rich in that absorbing species and a vapor-like phase dilute in it. To examine it closely, we plot in Fig. 4 the density profiles of nanoparticles normalized by their bulk concentrations for $\beta\epsilon_{AA}$s corresponding to Fig. 2 at $\rho^* = 5.1$ and $\rho^* = 6.1$. What is revealing in the plot at $\rho^* = 6.1$ is while for $\beta\epsilon_{AA}$ values up to 4, $\rho_n(z)/\rho_n^b$ decays to 1 far from the wall as is expected, for $\beta\epsilon_{AA} = 5$, $\rho_n(z)/\rho_n^b$ saturates to a significantly higher value ($\approx$72). This discrepancy between the bulk concentration seen in the calculation and the bulk concentration input into the calculation is due to the fact that there is phase separation in the bulk under increased self-interaction between nanoparticles as was conjectured before. To support this thesis, we show in Fig. 5 the vapor-liquid phase diagram of the bulk system. At $\beta\epsilon_{AA} = 5.0$, the vapor phase

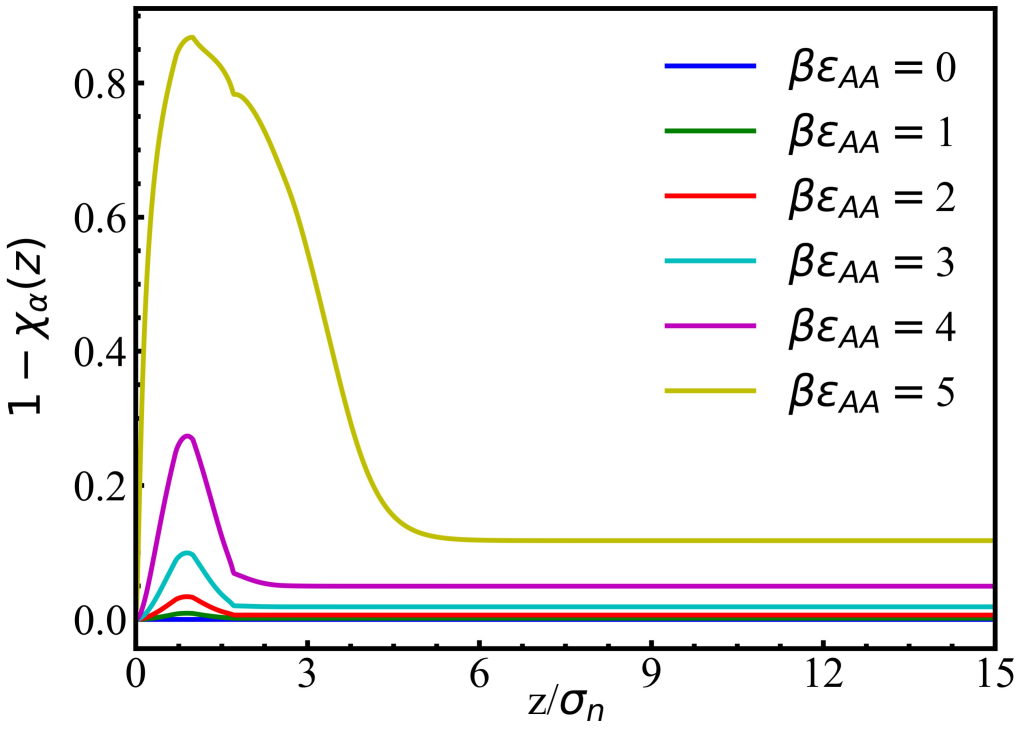

Figure 3: Fraction of associated nanoparticle functional groups as a function of distance from the surface for different nanoparticle self-association strengths ($\beta\epsilon_{AA}$). The chosen concentration ($\rho^* = 5.1$) is just before the wetting transition for $\beta\epsilon_{AA} = 5.0$ in Fig. 2.

composition, located on the left branch of the phase diagram, is $\rho^* = 6.13$. Since the input bulk composition into the computation here, 6.1, is near this value, there is phase separation. Please note that this value is in the single phase region. However, the distance from the two-phase region boundary is quite small and hence, we posit that this premature phase separation was induced by the surface, which has been shown to give rise to phase behavior different from bulk phase behavior [29]. The composition of the liquid phase is 439.6, which agrees with the factor of increase observed in the density profile. For lower values of ϵ_{AA}, the studied composition range is far from the binodal curve and hence no phase separation is observed. It is also seen that the segregated region near the surface extends much deeper into the bulk for the phase separated fluid than the range of particle-wall attraction. Such behavior in density profiles was also observed in polymer adsorption

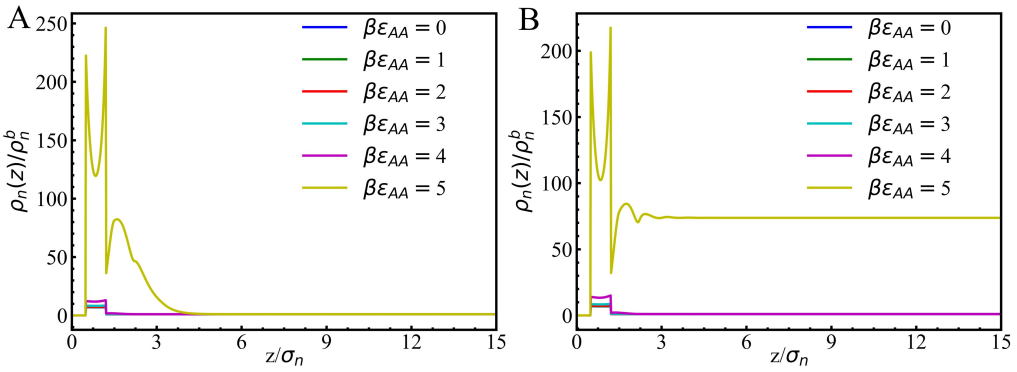

Figure 4: Concentration profiles of nanoparticles normalized by their bulk concentration for different nanoparticle self-association strengths ($\beta\epsilon_{AA}$). The left panel is at the density preceding the wetting transition ($\rho^* = 5.1$) and the right panel is just after the wetting transition ($\rho^* = 6.1$).

onto a surface under poor solvent conditions [28]. Our work shows that increased association has the same effect as worsening solvent quality, driving the system towards phase separation and subsequent wetting.

3.2. Adsorption in nanoparticle-polymer system

Next, we examine the effect of the association strength between polymer functional groups and nanoparticle functional groups ($\beta\epsilon_{AB}$) on adsorption. Fig. 6 shows the variations of adsorbed nanoparticle amount (panel A) and adsorbed monomer amount (panel B) for a mixture containing same amounts of both species by weight ($\frac{\rho_P^b \sigma_P^3}{\rho_n^b \sigma_n^3} \approx 0.1$) for $\beta\epsilon_{AA} = 2.0$. and $N_p = 10$. It is clear from the plots that increasing ϵ_{AB} inhibits nano-particle adsorption and this suppressing effect is appreciable at high nanoparticle concentrations. For monomer adsorption, we find that the adsorption amount depends non-monotonically on ϵ_{AB} in which adsorption is maximized at intermediate values of ϵ_{AB}. Additionally, for low ϵ_{AB} values, there is desorption of monomers and later there is adsorption as ϵ_{AB} increases. It is also evident in the plots that while in the studied concentration range, Γ_n rises with increasing ρ^*, Γ_m first increases and then decreases.

Polymer adsorption, in addition to translational entropic cost of confinement, involves a conformational entropic cost of confinement. While this additional restriction is operative on nanoparticle clusters, every monomer

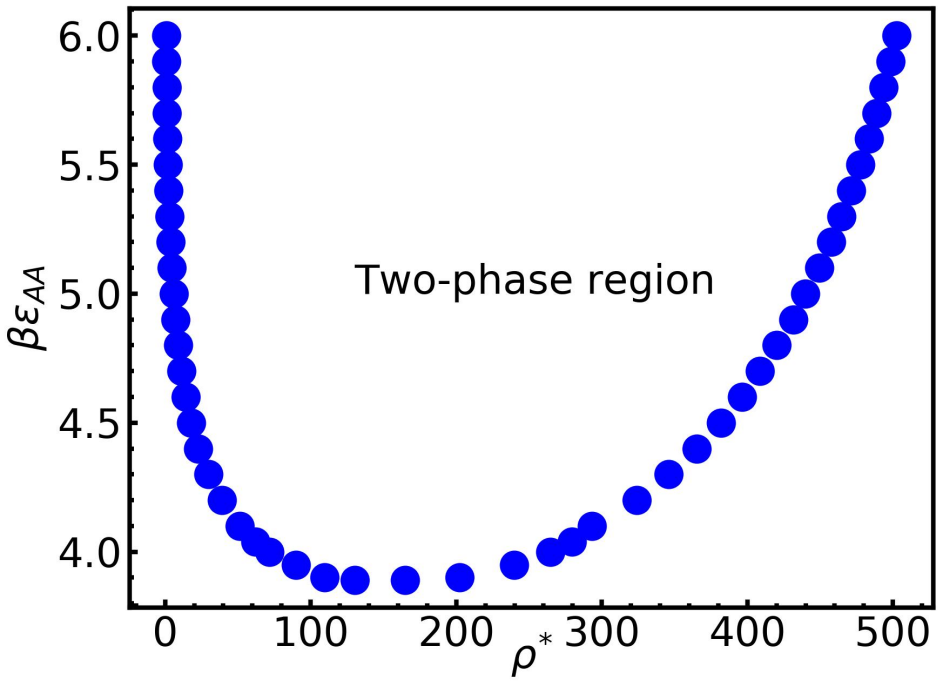

Figure 5: Bulk phase diagram $\beta\epsilon_{AA}$ vs ρ^* for the studied associative nanoparticle system.

making up these clusters experiences attraction with the surface. This overcomes the conformational entropic cost. Hence, as ρ^* increases, Γ_n increases due to increased cluster formation. However, in polymer chains of our model, only the end monomer is attracted to the surface, meaning the counteracting force against the loss of conformational entropy is low. This coupled with high excluded volume interactions resulting from high nanoparticle concentration near the wall makes Γ_m either decrease or increase and then saturate with increasing ρ^*. Returning to the dependence of Γ_n and Γ_m on ϵ_{AB}, there is a competition between nanoparticle-nanoparticle association and nanoparticle-polymer association. And, as is obvious, increasing ϵ_{AB} makes the latter stronger, which decreases the aggregate size of nanoparticle clusters, leading to decreased adsorption. As for the trend of Γ_m vs ϵ_{AB} however, the reasons are not immediately obvious to us. We believe initially at low ϵ_{AB}, the loss of conformational entropy suppresses adsorption. However, as ϵ_{AB} becomes

significant, there is increased association between nanoparticles and polymer chains and as a consequence, polymer chains are dragged towards the interface by nanoparticles. It should be noted that with increasing ϵ_{AB}, the concentration of nanoparticles near the interface is also decreasing, which is negating their above-mentioned adsorption-boosting cooperativity effect. At very high ϵ_{AB}, the latter overwhelms the former and a decrease in Γ_m is observed.

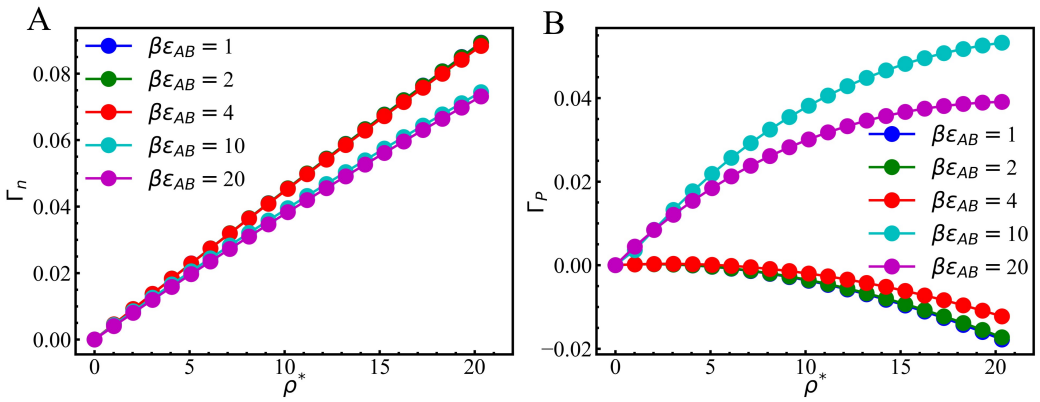

Figure 6: The variation of (A) adsorbed nanoparticles and (B) adsorbed monomers as a function of nanoparticle concentration for different nanoparticle-polymer interaction strengths ($\beta\epsilon_{AB}$) at $\beta\epsilon_{nS} = 2.0$. The amount of monomer in concentration by weight in the bulk solution is the same as the nanoparticle amount.

In order to strengthen the above argument, we analyze the distance-variation of fraction of A groups associating with A groups (x_{AA}) and the fraction of A groups associating with B groups (x_{AB}). Since the quantities in the association free energy expression (χ_A and χ_{AB}) are the unreacted fractions of A and B groups, we propose an ad hoc way of computing x_{AA} and x_{AB} based on stoichiometry according to the following relation:

$$\rho_B(z)[1 - \chi_{AB}(z)] = 4\rho_n(z)x_{AB}(z) \tag{20}$$

The left hand side in the equation gives the density of reacted B groups and that is equated to the density of nanoparticle groups bonding with B. The factor of 4 is to account for the number of functional groups on a nanoparticle. As a note of caution, we add that this relationship is only approximate since the equation is local in nature while the association free energy expression

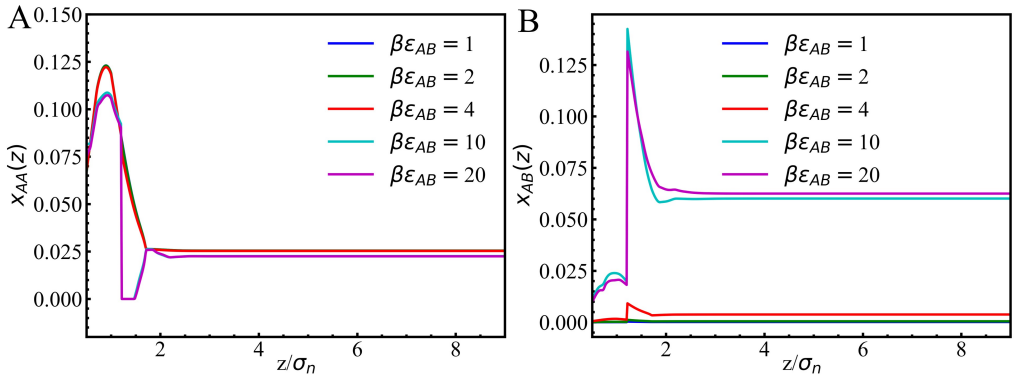

Figure 7: (A) Fraction of nanoparticle functional groups bonded to groups of the same type as a function of distance, (B) Fraction of nanoparticle functional groups bonded to polymer functional groups as a function of distance for different nanoparticle-polymer association strengths ($\beta\epsilon_{AB}$) at $\rho^* = 20.3$ and $\beta\epsilon_{nS} = 2.0$.

is embedded with non-local quantities through weighted densities. However, qualitatively the trends on the effect of inter-association should be reasonably accurate. Once $x_{AB}(z)$ has been obtained, $x_{AA}(z)$ is computed from the relation: $x_{AA}(z) = 1 - \chi_A(z) - x_{AB}(z)$. Fig. 7 shows the distance variation of $x_{AA}(z)$ and $x_{AB}(z)$ and it is evident that increasing ϵ_{AB} decreases $x_{AA}(z)$ by increasing $x_{AB}(z)$. It is also seen, that $x_{AB}(z)$ is peaked near the surface due to increased concentration of both species in that region and there is a slight decrease in it in going from 10.0 to 20.0 in $\beta\epsilon_{AB}$. This is consistent with the trend in Fig. 6, which shows the peak in Γ_n is attained at $\beta\epsilon_{AB} = 10.0$.

Chain length is an important parameter in polymer thermodynamics since it directly affects the conformational and translational entropic parts of the system free energy. In the adsorption context, in the past, longer polymer chains were shown to adsorb more onto an attractive surface than shorter polymer chains for the same bulk monomer concentration [28]. Similarly, in two component systems involving a solvent, short polymer chains mix better with the solvent than long polymers [30]. To see how chain length features in mediating the adsorption of a dissimilar component, we plot the variation of adsorption isotherm for nanoparticles for different polymer chain lengths (N_P) in Fig. 8 at two different relative strengths of cross-association. Here, we keep the polymer chain concentration, hence the number of B groups, constant at the nanoparticle number density so as to isolate the effect arising

from chain lengths of polymers. It is seen in the plots that Γ_n decreases with decreasing N_P at both values of $\beta\epsilon_{AA}$. Additionally, shorter chains also delay the onset of wetting transition as is shown in the right panel (b). Association between nanoparticles and the functional end monomer of the polymer requires the polymer chain to be locked in a limited number of conformations, which carries an entropic penalty cost. This entropic cost is lower for short chains than for long chains due to the smaller number of accessible conformations to short chains in their unbound states. This decreased cost leads to higher amounts of association between nanoparticles and polymers for short chains, leading to enhanced suppression of nanoparticle adsorption. This claim is supported by Fig. 9, which shows $x_{AB}(z)$ to be decreasing with increasing degree of polymerization both in the bulk and near the surface. Additionally, the conformational entropic penalty of confinement is small for short chains, which enhances their crowding near the surface compared to long chains. This further amplifies desorption of nanoparticles through both excluded volume effects and breakage of nanoparticle clusters near the surface.

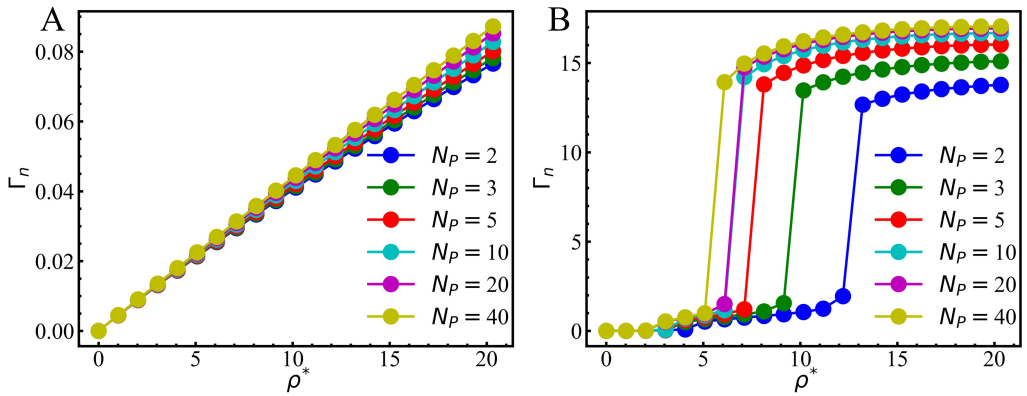

Figure 8: Nanoparticle adsorption isotherms for different polymer chain lengths. The left panel is for low self-association strengths ($\beta\epsilon_{AA} = 2.0$) and the right panel for high self-association strengths ($\beta\epsilon_{AA} = 5.0$). The inter-association strength was fixed at $\beta\epsilon_{AB} = 10.0$.

From the above discussions, it is clear that characteristics of the polymer chain plays a significant role in nanoparticle adsorption through its interplay with chemical association and the cooperativity resulting therefrom. To highlight this aspect further, we vary the polymer-surface affinity (ϵ_{BS}) and

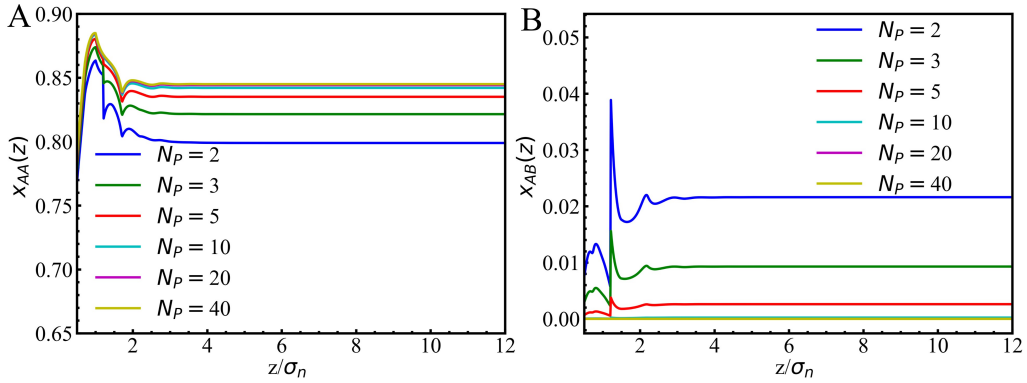

Figure 9: The variation of (A) self-association (B) inter-association of nanoparticle functional groups for different lengths of polymer at $\rho^* = 20.3, \beta\epsilon_{AA} = 2.0$ and $\beta\epsilon_{AB} = 10.0$. This parameter set corresponds to the left panel in Fig. 8.

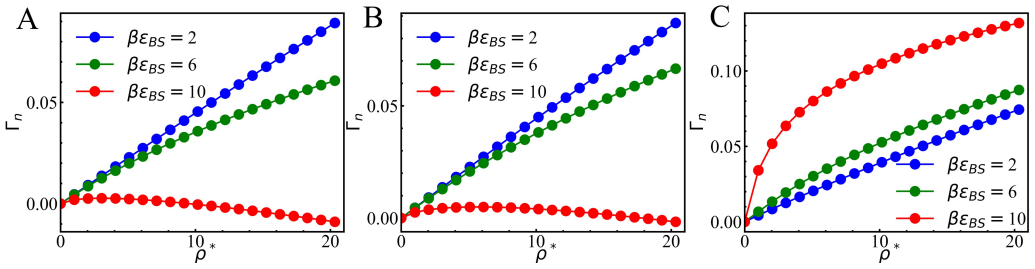

Figure 10: The variation of nanoparticle adsorption (Γ_n) with polymer surface affinity ($\beta\epsilon_{BS}$) for three different nanoparticle-polymer affinities ($\beta\epsilon_{AB} = A$) 2.0 B) 5.0 C) 10.0) at $\beta\epsilon_{AA} = 2.0$ and $\beta\epsilon_{nS} = 2.0$.

see how that couples with nanoparticle adsorption. Intuitively speaking, just as ϵ_{nS} enhances nanoparticle adsorption, increasing ϵ_{BS} would inhibit it by preferentially pushing polymer chains towards the wall over nanoparticles. However, our results deviate from this expected trend. Fig. 10 plots the effect of ϵ_{BS} on Γ_n at three different ϵ_{AB}s at constant ϵ_{AA} and ϵ_{nS}. It is seen in the plots that for low ϵ_{AB} (panels A and B), increasing ϵ_{BS} suppresses nanoparticle adsorption. However, for sufficiently high ϵ_{AB} (panel C), increasing ϵ_{BS} has an enhancing effect on Γ_n. These opposing effects of ϵ_{BS} can be explained through cooperativity between nanoparticle and polymer. At low ϵ_{AB}, most polymers are unassociated. Hence, increasing ϵ_{BS} simply drives the chains towards the surface, which excludes nanoparticles from the

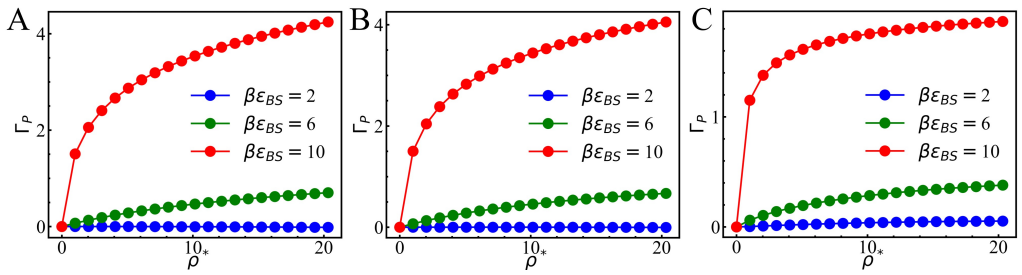

Figure 11: The variation of monomer adsorption (Γ_m) with polymer surface affinity ($\beta\epsilon_{BS}$) for three different nanoparticle-polymer affinities ($\beta\epsilon_{AB}$ = *A)* 2.0 *B)* 5.0 *C)* 10.0) at $\beta\epsilon_{AA} = 2.0$ and $\beta\epsilon_{nS} = 2.0$.

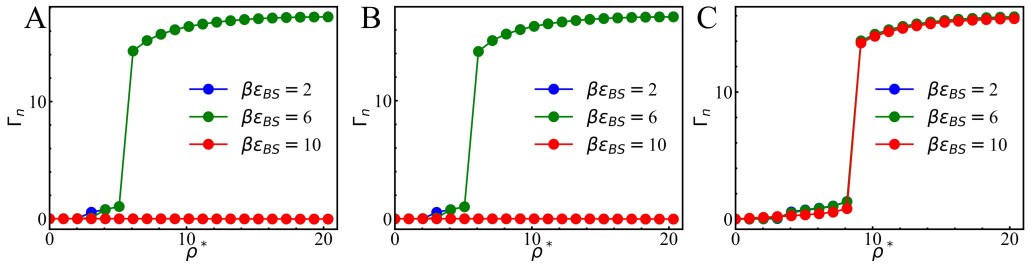

Figure 12: The variation of nanoparticle adsorption (Γ_n) with polymer surface affinity ($\beta\epsilon_{BS}$) for three different nanoparticle-polymer affinities ($\beta\epsilon_{AB}$) at $\beta\epsilon_{AA} = 5.0$ and $\beta\epsilon_{nS} = 2.0$.

surface region due to packing effects. However, at high ϵ_{AB}, most polymers are associated with nanoparticles. This implies that when they deposit near the surface with increasing ϵ_{BS}, the nanoparticles are swept with them towards the surface. Additionally, unlike the previous case, excluded volume effects are not significant here since the absolute values of adsorbed monomer amount are smaller at higher ϵ_{AB} than at lower ϵ_{AB}, as shown in Fig. 11. Both these phenomena concertedly explain increased Γ_n at enhanced ϵ_{BS} values. However, the above effect is weakened when there is sufficient self-association (see plots for $\beta\epsilon_{AA} = 5$ in Fig. 12) and one recovers suppressing effects of ϵ_{BS}.

3.3. Effect of surface chemistry

All the results presented so far are for a formalism that is based on the assumption that the attraction strength between the surface and the particles is

insensitive to the adsorption amount. This assumption is valid when the attraction is physical, such as that due to van der Waals forces or the number of surface sites causing adsorption is large compared to the number of adsorbing species. However, in many real systems, adsorption involves pair interactions such as acid-base pair formation [31, 32]. Here, the surface sites become unavailable for further association once they have been occupied by adsorbing species. This saturation of surface sites has been studied in the past in the context of dissociable surfaces and ion distribution around them[33, 34]. Here, the surface groups in their dissociated form interact electrostatically with ions in the solution, providing the driving force for their accumulation near the interface and once these surface groups react with some of the accumulated ions, they no longer contribute to the electrostatic potential. Along the lines of those theories, here we model adsorption as a chemical reaction ($S + N \rightarrow NS$), characterized by an equilibrium constant(K^o_{NS}). Since the goal is solely to identify the modification brought about by saturation in associative systems, we restrict ourselves to only nanoparticle adsorption. The effect of surface site saturation enters the driving force for adsorption through the effective one body potential exerted by the surface, which is given by:

$$V_i^{ext}(\mathbf{r}) = \begin{cases} \infty, & z < \sigma_i/2, \\ -\epsilon_{is}(1 - f_{NS}), & \sigma_i/2 \leq z \leq \delta_i, \\ 0, & z > \delta_i \end{cases} \tag{21}$$

Here, ϵ_{iS} is the strength of the attraction exerted by all surface species combined. f_{NS} is the fraction of associated sites, and hence, the factor $(1 - f_{NS})$ implies that only unassociated sites contribute to $V_i^{ext}(\mathbf{r})$. f_{NS} is computed through a law of mass action relationship

$$\frac{f_{NS}}{\bar{\rho}_N a_N (1 - f_{NS})} = K^o_{NS} \tag{22}$$

where a_N is the volume of nanoparticles and $K^o_{NS} = \exp(-\beta(\mu^o_{NS} - \mu^o_S - \mu^o_n))$ is the equilibrium constant of association. $\bar{\rho}_N(z)$ is the average of nanoparticle density over the attractive layer ($\sigma_i/2 \leq z \leq \delta_i$). Here, we would like to inform the reader that the above formulation connects f_{NS} and $\rho_n(z)$ implicitly i.e. while deriving the expression for $\rho_n(z)$, we do not differentiate the external potential with respect to $\rho_n(z)$. This is done to keep the parameters in the model to a minimum and focus on the effects arising from saturation of the interface. As for the expression for f_{NS}, we have not explicitly taken

into account the effect of surface group density to avoid complicating the picture and focus purely on the effect of saturation. However, for the sake of completeness, we present a more complete treatment of interface saturation in the supplementary section. Returning to Eqn. 22, the density in the denominator in charge regulation theories is usually the density at contact with the surface. Here, in our case, we take this to be the average density over the attractive layer assuming that all nanoparticles in this layer are capable of participating in the association. Additionally, the variations in the choice of ρ_N only shift the dependence of f_{NS} on ρ^* quantitatively and has the same effect as changing K^o_{NS}. Now, $\bar{\rho}_N(z)$ and $V^i_{ext}(z)$ are interdependent; so f_{NS} and $\rho_N(z)$ must be determined self-consistently. Typically, the calculation is started with a f_{NS} value corresponding to the bulk nanoparticle concentration, which sets the initial $V_i^{ext}(\mathbf{r})$. Using this external potential, the nanoparticle density profile is solved for with classical density functional theory. From the density profile, f_{NS} is computed again using Eq. 22 and the process is repeated till the difference between f_{NS} values from two successive iterations decreases to below 0.0001.

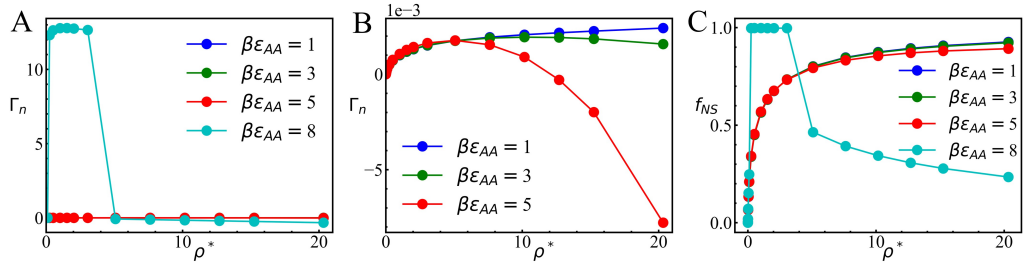

Figure 13: The variation of nanoparticle adsorption isotherms (A and B) with self-association energy (ϵ_{AA}) for a saturable surface at $\beta\epsilon_{nS} = 2.0$. The rightmost panel (C) shows the corresponding associated fraction of surface groups.

Panels A and B in Fig. 13 show nanoparticle adsorption isotherms under various self-association strengths for $K^o_{AS} = 1000$ and $\beta\epsilon_{nS} = 2.0$. This equilibrium constant value corresponds to approximately $\rho^* = 0.75$ for fifty percent association ($f_{NS} = 0.5$) of the bulk fluid. The choice of this value of K^o_{AS} is arbitrary. Nevertheless, other values of K^o_{AS} do not affect the results other than shifting the curves along the composition axis. The corresponding curves for the dependence of f_{NS} on concentration are shown in panel C in the same figure. There are two regimes noticed in adsorption isotherms in terms of Γ_n vs ϵ_{AA} dependence. In the first regime, which occurs

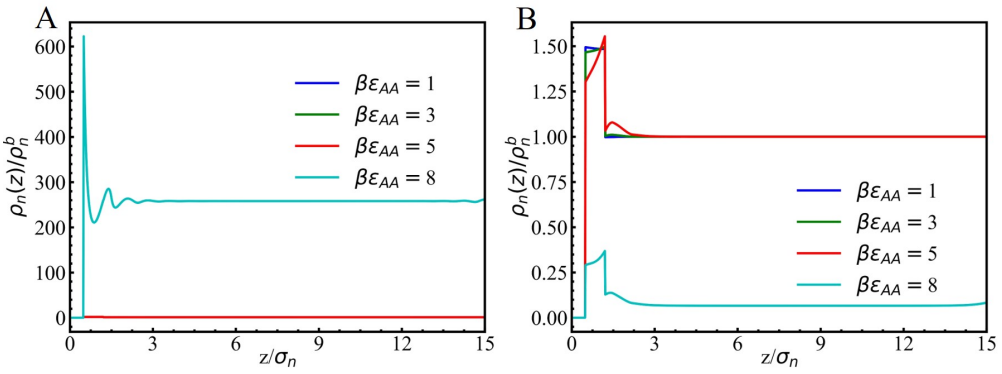

Figure 14: The variation of nanoparticle adsorption isotherms (A and B) with self-association energy (ϵ_{AA}) for a saturable surface at $\beta\epsilon_{nS} = 2.0$. The rightmost panel (C) shows the corresponding associated fraction of surface groups.

at low concentrations, Γ_n increases with concentration and shows negligible dependence on ϵ_{AA} with the corresponding curves merging together. This behavior is in contrast with the physical adsorption case, where there is a positive correlation between Γ_n and ϵ_{AA}. As the concentration increases, in the second regime, Γ_n decreases. The crossover concentration is attained earlier for higher values of $\beta\epsilon_{AA}$s and the decrease following it is steeper. As bulk concentration increases, there is accumulation of nanoparticles near the surface in a manner similar to physical adsorption. However, this process also coincides with weakening of the external potential due to the filling of adsorption sites, which reduces the driving force for adsorption. This latter factor further depletes the surface region of nanoparticles. This hypothesis is corroborated by the corresponding f_{NS} vs concentration curves. Here, f_{NS} attains saturation at high concentrations of nanoparticle. This means there is no driving force for adsorption and this zero driving force coupled with high excluded volume pressure of segregated nanoparticles leads to some of the sites undergoing unbinding, releasing nanoparticles into the bulk. This is reflected in a decrease in f_{NS} with concentration. Another noteworthy feature evident in these curves is that at high ϵ_{AA}, the adsorption isotherm displays a drop at high concentrations. To delve into the structural origin of this behavior, we give in Fig. 14 the nanoparticle density profiles just before and after the drop in Γ_n. In both the plots, the normalized density values for $\beta\epsilon_{AA} = 1, 3, 5$ approach 1 far from the surface while for $\beta\epsilon_{AA} = 8$, there

is an increase by factor of 255 before the drop and a decrease by a factor of 10 after the drop. This increase is characteristic of wetting as was discussed before. The decrease is more interesting since the composition corresponds to the vapor side of the phase diagram. Since both the liquid-side and the vapor-side profiles have the same grand potential in the two-phase region of the phase diagram, we believe the transition from liquid-rich profile to vapor-rich profile is due to one profile being closer to the initial guess than the other in the numerical solution of the equations at a given concentration and is not indicative of any phase transition. Nevertheless, this decrease in f_{NS} for non-wetting conditions instead of saturation emphasizes the self-consistent mechanism between adsorption and surface binding.

4. Conclusions

A classical density functional theory has been used to study the behavior of associating nanoparticles and associating polymers in the vicinity of an attractive wall. This system has relevance in many scientific and industrial processes, such as the use of resin to circumvent asphaltene deposition in reservoirs. In our study, enhanced association strength of nanoparticles was seen to promote their deposition. On the other hand, increasing the cross-association strength between nanoparticle and polymer chain functional groups suppressed nanoparticle adsorption through breakage of nanoparticle clusters. The length of the polymer chains was also found to be an important factor with small chains preventing adsorption more effectively than long chains. These observed trends were explained through an analysis of association as well as density profiles, which revealed an interplay between entropic and energetic molecular forces. An interesting non-intuitive consequence of this interplay was enhancement of nanoparticle adsorption with increasing polymer-surface affinity under high cross-association strengths. Finally, the formalism was adapted to incorporate the case of saturation of the surface functional groups and in this case, we found suppressed nanoparticle adsorption compared to the non-saturable case along with a reversal in the effect of nanoparticle self-association strength.

The parameter space for the nanoparticle-polymer adsorption problem is quite wide and in our work, we have covered only a limited number of parameters. Possible future investigations could include an exhaustive scan of the parameter space, the effect of solvent quality through van der Waals/dispersive interactions, the adsorption behavior in a pore, etc. Intu-

itively, we believe dispersive interactions will exhibit similar results to associative interactions though the presence of two competing factors, the reduced interaction strength and the long range nature of the interaction, might either magnify or lessen the effect. Another direction might involve checking the validity of lateral homogeneity assumption through a three dimensional calculation. This is believed to have considerable influence in the case of saturable adsorption. To summarize, our work takes the first step towards developing a general theoretical understanding to help practitioners in the petroleum industry in developing insights into physical principles underlying asphaltene-deposition induced problems as well as in guiding the design of polymers to circumvent them.

5. Acknowledgements

This work is financially supported by the American Chemical Society Petroleum Research Fund (PRF# 60868-ND9). We also acknowledge additional support from the National Science Foundation under Grant no. DGE-1326120.

Appendix A. Derivation of association fraction

To derive an expression for f_{NS}, we add to the grand potential ($\beta\Omega$) the chemical free energy of association:

$$\begin{aligned}\beta f_{chem} = {} & \sigma f_{NS}[\log(\sigma f_{NS} a_S) - 1] + \sigma(1 - f_{NS})[\log(\sigma(1 - f_{NS})a_S) - 1] \\ & + \sigma f_{NS}\mu^o_{NS} \\ & + \sigma(1 - f_{NS})\mu^o_S + \int dz \mu^o_n \rho_n(z) - \sigma f_{NS}\mu_n\end{aligned} \tag{A.1}$$

where σ is the surface group density and a_S is a multiplicative constant to make the term inside the logarithm dimensionless and has the dimension of area. The first two terms give the mixing entropy of associated and unassociated surface species. The next three terms are the standard state free energies of associated and unassociated surface groups and nanoparticles, respectively. The final term is the chemical potential term for the nanoparticles to account for associated nanoparticles, which are represented by NS in the

reaction $S + N \rightarrow NS$. ρ_n and f_{NS} are determined by minimizing $\beta\Omega$ with respect to them. The resulting expressions for the two quantities are

$$\rho_n(z)a_n = \exp(\beta(\mu_n - \mu_n^o))\exp(-w_n(z)) \tag{A.2}$$

$$\begin{aligned}\frac{f_{NS}}{1-f_{NS}} &= \exp(\beta(\mu_n - \mu_n^o))K_{AS}^o\exp(\frac{1}{\sigma}\int dz\rho_n(z)\frac{dV_{ext}}{df}) \\ &= \exp(\beta(\mu_n - \mu_n^o))K_{AS}^o\exp(-\frac{L}{\sigma}\bar{\rho_n}\epsilon_{iS})\end{aligned} \tag{A.3}$$

where L is the width of the attractive layer. Substituting Eqn. A.2 into Eqn. A.3, we get

$$\frac{f_{NS}}{1-f_{NS}} = \frac{\rho_N(z)a_N}{\exp(-w_n(z))}K_{AS}^o\ \exp(-\frac{L}{\sigma}\bar{\rho_n}\epsilon_{iS}) \tag{A.4}$$

The denominator in the first term on the right hand side of the above equation captures explicit correlation effects and the last term explicit self-regulation effect. This self-regulation effect has negligible contribution if the surface group density, σ, is very high. Usually, these explicit terms are ignored in charge-regulation theories, which leads to Eqn. 22, and correlation is captured indirectly through the density profiles of free species and the electrostatic field.

References

[1] J. J. Adams, Asphaltene adsorption, a literature review, Energy & Fuels 28 (2014) 2831–2856.

[2] R. Syunyaev, R. Balabin, I. Akhatov, J. Safieva, Adsorption of petroleum asphaltenes onto reservoir rock sands studied by near-infrared (nir) spectroscopy, Energy & Fuels 23 (2009) 1230–1236.

[3] J. Buckley, Y. Liu, S. Monsterleet, Mechanisms of wetting alteration by crude oils, SPE journal 3 (1998) 54–61.

[4] C. Drummond, J. Israelachvili, Fundamental studies of crude oil–surface water interactions and its relationship to reservoir wettability, Journal of Petroleum Science and Engineering 45 (2004) 61–81.

[5] J. L. Mendoza de la Cruz, F. J. Arguelles-Vivas, V. Matias-Perez, C. d. l. A. Durán-Valencia, S. Lopez-Ramirez, Asphaltene-induced precipitation and deposition during pressure depletion on a porous medium: an

experimental investigation and modeling approach, Energy & Fuels 23 (2009) 5611–5625.

[6] I. Gawel, D. Bociarska, P. Biskupski, Effect of asphaltenes on hydroprocessing of heavy oils and residua, Applied Catalysis A: General 295 (2005) 89–94.

[7] J. A. Koots, J. G. Speight, Relation of petroleum resins to asphaltenes, Fuel 54 (1975) 179–184.

[8] J. Speight, Petroleum asphaltenes-part 1: Asphaltenes, resins and the structure of petroleum, Oil & gas science and technology 59 (2004) 467–477.

[9] M. R. Gray, R. R. Tykwinski, J. M. Stryker, X. Tan, Supramolecular assembly model for aggregation of petroleum asphaltenes, Energy & Fuels 25 (2011) 3125–3134.

[10] C. A. Franco, M. M. Lozano, S. Acevedo, N. N. Nassar, F. B. Cortés, Effects of resin i on asphaltene adsorption onto nanoparticles: A novel method for obtaining asphaltenes/resin isotherms, Energy & Fuels 30 (2016) 264–272.

[11] S. Tazikeh, A. Shafiei, T. Yerkenov, A. Abenov, N. Seitmaganbetov, T. S. Atabaev, A systematic and critical review of asphaltene adsorption from macroscopic to microscopic scale: Theoretical, experimental, statistical, intelligent, and molecular dynamics simulation approaches, Fuel 329 (2022) 125379.

[12] N. N. Nassar, Asphaltene adsorption onto alumina nanoparticles: kinetics and thermodynamic studies, Energy & Fuels 24 (2010) 4116–4122.

[13] O. E. Medina, C. Caro-Vélez, J. Gallego, F. B. Cortés, S. H. Lopera, C. A. Franco, Upgrading of extra-heavy crude oils by dispersed injection of nio–pdo/ceo2$\pm\delta$ nanocatalyst-based nanofluids in the steam, Nanomaterials 9 (2019) 1755.

[14] J. Wu, Density functional theory for chemical engineering: From capillarity to soft materials, AIChE journal 52 (2006) 1169–1193.

[15] J. Wu, J. M. Prausnitz, A. Firoozabadi, Molecular thermodynamics of asphaltene precipitation in reservoir fluids, AIChE journal 46 (2000) 197–209.

[16] J. Wu, J. M. Prausnitz, A. Firoozabadi, Molecular-thermodynamic framework for asphaltene-oil equilibria, AIChE journal 44 (1998) 1188–1199.

[17] C. J. Segura, W. G. Chapman, Associating fluids with four bonding sites against solid surfaces: Monte carlo simulations, Molecular Physics 86 (1995) 415–442.

[18] C. J. Segura, J. Zhang, W. G. Chapman, Binary associating fluid mixtures against a hard wall: density functional theory and simulation, Molecular Physics 99 (2001) 1–12.

[19] S. Tripathi, W. G. Chapman, A density functional approach to chemical reaction equilibria in confined systems: application to dimerization, The Journal of chemical physics 118 (2003) 7993–8003.

[20] T. Zeitler, J. Greathouse, R. Cygan, J. Fredrich, G. Jerauld, Molecular dynamics simulation of resin adsorption at kaolinite edge sites: Effect of surface deprotonation on interfacial structure, The Journal of Physical Chemistry C 121 (2017) 22787–22796.

[21] Y. Rosenfeld, Free-energy model for the inhomogeneous hard-sphere fluid mixture and density-functional theory of freezing, Physical review letters 63 (1989) 980.

[22] D. Cao, J. Wu, Microstructure of block copolymers near selective surfaces: Theoretical predictions and configurational-bias monte carlo simulation, Macromolecules 38 (2005) 971–978.

[23] Y.-X. Yu, J. Wu, A fundamental-measure theory for inhomogeneous associating fluids, The Journal of chemical physics 116 (2002) 7094–7103.

[24] W. G. Chapman, K. E. Gubbins, G. Jackson, M. Radosz, New reference equation of state for associating liquids, Industrial & engineering chemistry research 29 (1990) 1709–1721.

[25] D. Cao, J. Wu, Surface forces between telechelic brushes revisited: The origin of a weak attraction, Langmuir 22 (2006) 2712–2718.

[26] E. Buenrostro-Gonzalez, C. Lira-Galeana, A. Gil-Villegas, J. Wu, Asphaltene precipitation in crude oils: Theory and experiments, AIChE Journal 50 (2004) 2552–2570.

[27] V. Sethuraman, M. McGovern, D. C. Morse, K. D. Dorfman, Influence of charge sequence on the adsorption of polyelectrolytes to oppositely-charged polyelectrolyte brushes, Soft Matter 15 (2019) 5431–5442.

[28] E. Y. Lin, A. L. Frischknecht, K. I. Winey, R. A. Riggleman, Effect of surface properties and polymer chain length on polymer adsorption in solution, The Journal of Chemical Physics 155 (2021) 034701.

[29] P. T. Cummings, H. Docherty, C. R. Iacovella, J. K. Singh, Phase transitions in nanoconfined fluids: The evidence from simulation and theory, AIChE journal 56 (2010) 842–848.

[30] M. Rubinstein, R. H. Colby, et al., Polymer physics, volume 23, Oxford university press New York, 2003.

[31] S. Dubey, M. Waxman, Asphaltene Adsorption and Desorption from Mineral Surfaces. SPE Res Eng 6 (3): 389–395, Technical Report, SPE-18462-PA. https://doi. org/10.2118/18462-PA, 1991.

[32] D. Dudášová, S. Simon, P. V. Hemmingsen, J. Sjöblom, Study of asphaltenes adsorption onto different minerals and clays: Part 1. experimental adsorption with uv depletion detection, Colloids and Surfaces A: Physicochemical and Engineering Aspects 317 (2008) 1–9.

[33] G. M. Ong, A. Gallegos, J. Wu, Modeling surface charge regulation of colloidal particles in aqueous solutions, Langmuir 36 (2020) 11918–11928.

[34] G. Trefalt, S. H. Behrens, M. Borkovec, Charge regulation in the electrical double layer: ion adsorption and surface interactions, Langmuir 32 (2016) 380–400.